Neutron scattering for surface characterization

J. Penfold

ISIS Facility, CLRC, Rutherford Appleton Laboratory, Chilton, Didcot, Oxon OX11 OQX, UK

The use of the specular reflection of neutrons to provide information on the structure of surfaces and interfaces is described. Through hydrogen/deuterium isotopic substitution the refractive index distribution at interfaces can be manipulated, and this makes the technique particularly powerful for the study of the adsorption of polymers, surfactants, proteins and mixtures at interfaces.

The technique has developed enormously in the last 10 years, and this will be illustrated with a range of recent examples from the scientific programme on the ISIS pulsed neutron source. Examples, which include the nature of polymer–polymer interfaces, and the adsorption of surfactants, proteins and polymers at different interfaces, will be used to illustrate the development towards the study of complex multi-component systems, 'buried' interfaces, and time-dependent phenomena, and in the use of complex environments.

Introduction

Specular neutron reflection provides information about inhomogeneities normal to an interface or surface[1]. The basis of a neutron reflection experiment is that the variation of specular reflectivity with Q (the wave vector transfer, defined as $Q = 4\pi \sin\theta/\lambda$, where θ is the glancing angle of incidence, and λ the neutron wavelength) is simply related to the composition or concentration profile in the direction normal to the surface or interface. In the kinematic approximation[2] the specular reflection can be written as

$$R(Q) = \frac{16\pi^2}{Q^2}|\rho(Q)|^2, \quad (1)$$

where $\rho(Q)$ is the one-dimensional Fourier transform of $\rho(z)$, the average scattering length density profile in the direction normal to the interface

$$\rho(Q) = \int_{-\infty}^{\infty} \rho(z)\exp(iQz)\mathrm{d}z, \quad (2)$$

and

$$\rho(z) = \sum_i N_i(z)b_i, \quad (3)$$

where N_i is the number density profile of species i and b_i is its scattering length.

The neutron refractive index is described as

$$n(z) \approx 1 - \sum_i N_i(z)b_i\lambda^2/2\pi. \quad (4)$$

In the exact definition of refractive index[1] there is an imaginary component, in addition to the real component. The imaginary component is related primarily to adsorption, and for the systems described in this review the adsorption cross-sections are negligable.

For most materials, as with X-rays, the neutron scattering lengths, b, are positive, and n is less than unity. This gives rise to total external reflection, in contrast to conventional light scattering. For neutrons and X-rays $1 - n \leq 10^{-4}$, and so the critical glancing angles for total reflection are small (0.1^o/Å for nickel, which has the largest value of Nb). This has important practical experimental consequences and measurements have to be made at grazing incidence using highly collimated beams. Perhaps the most important aspect of the technique is that hydrogen and deuterium have vastly different scattering powers, which are of different sign (b for H is -0.374×10^{-12} and for D is 0.6674×10^{-12} cm^{-1}). This means that for organic systems H/D isotopic substitution can be used to manipulate the refractive index distribution at the surface or interface, whilst leaving the chemistry essentially unaltered. By selective deuteration particular features or components at the interface or surface can be highlighted or masked, and it is this selectivity which makes the technique so powerful.

The essence of a specular reflection measurement is to measure the specular reflectivity as a function of wave vector transfer, Q, perpendicular to the surface or interface. This can be achieved in two different ways; either by using a single monochromatic wavelength and varying the grazing angle of incidence, or by using a fixed angle of incidence and a range of wavelengths (a 'white beam') which are sorted by time of flight. The latter approach is most suited to pulsed neutron sources, and the data reported in this review were measured on the SURF (ref. 3) and CRISP (ref. 4) reflectometers on the ISIS pulsed neutron source (Figure 1) in this way.

More experimental details of the method of specular neutron reflection can be found elsewhere[1–4]. Typically measurements are made at grazing angles of incidence in the range 0.25 to 1.8^o, using neutrons in the wavelength

e-mail: J.Penfold@rl.ac.uk

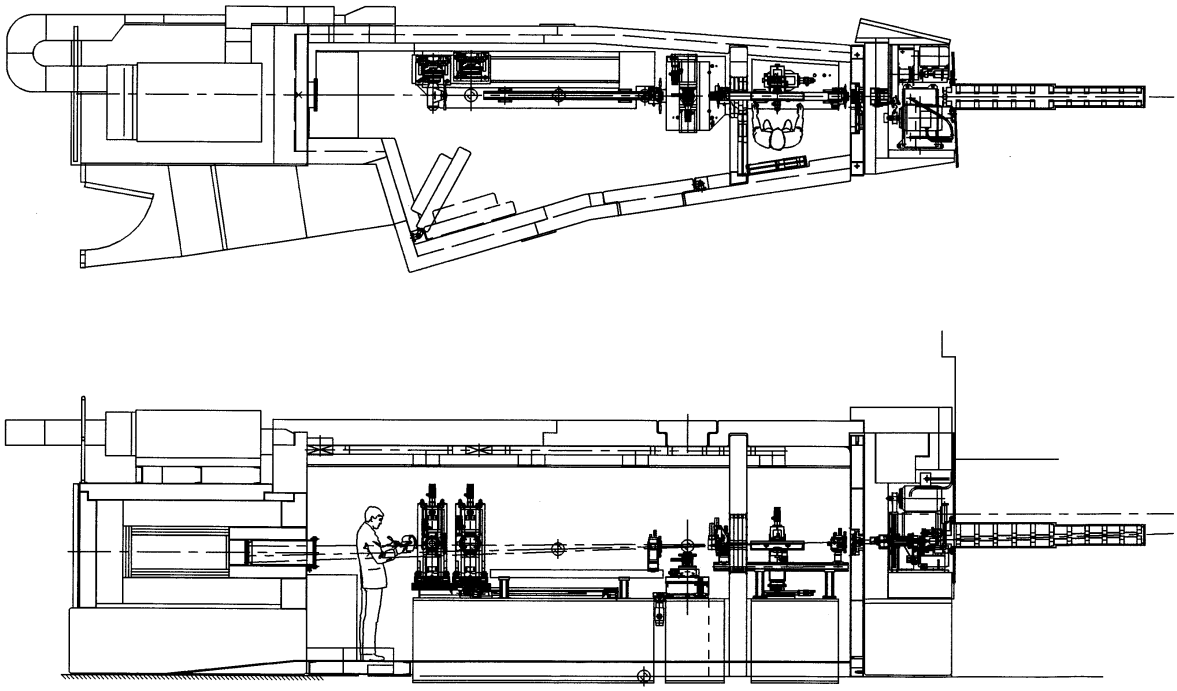

Figure 1 *a*. Schematic diagram of the layout of the SURF reflectometer at the ISIS pulsed neutron source.

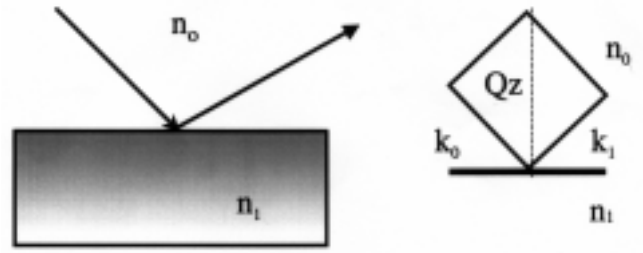

Figure 1 *b*. Scattering geometry for specular neutron reflection at grazing incidence.

range 1 to 7 Å to cover a Q range of 0.008 to 0.5 $Å^{-1}$. The incident beam is highly collimated in the z-direction to give values of $\Delta Q/Q$ typically from 2 to 5%. Vertical and horizontal slits, in the ranges 0.2 to 3.0 mm and 10.0 to 40 mm, provide sample illumination area in the range 1.0 to 100 cm^2. Measurement times vary in the range of tens of seconds to up to 2 h; and are highly dependent upon the particular system being studied. Measurements can be made from total reflection (at low Q) to reflectivities $\leq 10^{-7}$ (at high Q). The reflectivity decays as Q^{-4} and the signal/noise at high Q is usually limited by sample dependent background, predominantly from incoherent scattering contributions.

Polymer films and interfaces

Polymer–polymer interfaces are an important area of study since the interfacial behaviour is fundamental to the bulk properties of the system. This is particularly true when two or more polymers are mixed to form a blend, but the interface also plays a dominant role in areas such as adhesion, welding, surface wetting and mechanical strength. To fully understand polymer behaviour in such applications, the interface must be characterized at a microscopic level. Through deuterium labelling the interface between otherwise indistinguishable polymers can be studied, and neutron reflectivity provides unprecedented details on interfacial width and shape[5]. In addition to the inherent interdiffusion between polymers at a polymer–polymer interface, the interface is further broadened by thermally-driven capillary waves. Capillary waves produce a measured interfacial width which varies logarithmically with film thickness. Xiao *et al.*[6] measured the interfacial width of the polymer for polystyrene (PS) and poly (methyl methacrylate). Using deuterated polystyrene (d-PS) and polystyrene film thickness in the range 20 to 5000 Å they confirmed the logarithmical dependence on film thickness, to provide a reliable way to extract the intrinsic interfacial width from such measurements.

The time dependence of the early stages of polymer interdiffusion at interfaces is indicative of the diffusion process. The normal approach to study such interdiffusion by neutron reflectivity is to use an 'anneal/quench' cycle; where the sample is heated for a given time above the glass transition temperature (Tg) of the polymer, then quenched rapidly to room temperature, after which the reflectivity profile is measured. This has proved to

be highly effective on a number of systems, but is difficult to apply when Tg is ~ room temperature, or for small molecule ingress into a polymer layer.

The ability to measure simultaneously a wide Q range at fixed geometry (angle of incidence) using the white beam time of flight method on a pulsed source and the fluxes now available in the SURF reflectometer at ISIS means that *in situ* real time reflectivity measurements are now possible. Bucknall *et al.*[7] have pioneered this approach for the measurement of polymer–polymer interdiffusion with a series of ground-breaking experiments with measurement times down to ≤ one minute for carefully optimized sample geometries. The reflectivity profile for such polymer bilayers is characterized by a series of interference fringes whose period is inversely related to the deuterated polymer film thickness which comprises half of the bilayer (Figure 2).

These fringes damp with increasing Q, and the rate of damping with Q is directly related to the polymer–polymer interfacial width. As the interdiffusion process proceeds the angle of incidence is altered to capture the region of reflectivity most sensitive to the interfacial width. For the h – PS/d – PS bilayer Bucknall *et al.*[7] were able to show that this approach was equivalent to the 'quench/anneal' cycling and measured reflectivity profiles at 5 min intervals. The data were consistent with a symmetrical error function interface characterizing the polymer interdiffusion. Below the reptation time, τ_R, the interfacial width followed a $t^{1/4}$ behaviour and above τ_R, $t^{1/2}$ (classical Fickian diffusion), consistent with theoretical predictions. Using a specially designed cell, based on the type of cell used for studying the liquid–solid interface (see later), they have demonstrated that the same approach can be used to study small molecule ingress. Data similar to that in Figure 2 have been obtained for the diffusion of oligomeric-styrene (OSt) into high molecular weight deuterated polystyrene (d-PS). Measurements were made at 5 minute intervals, and during the course of the experiment the grazing angle of incidence was decreased from 0.8 to 0.5° to move the window of measurements to lower Q as the interface progressively broadened. In this case the data were consistent with a highly asymmetrical interfacial profile, and could be described by two error functions of width w_1, w_2, which were discontinuous about the interface centre x_0. The time dependence of these parameters is shown in Figure 3. The width of the d-PS side of the

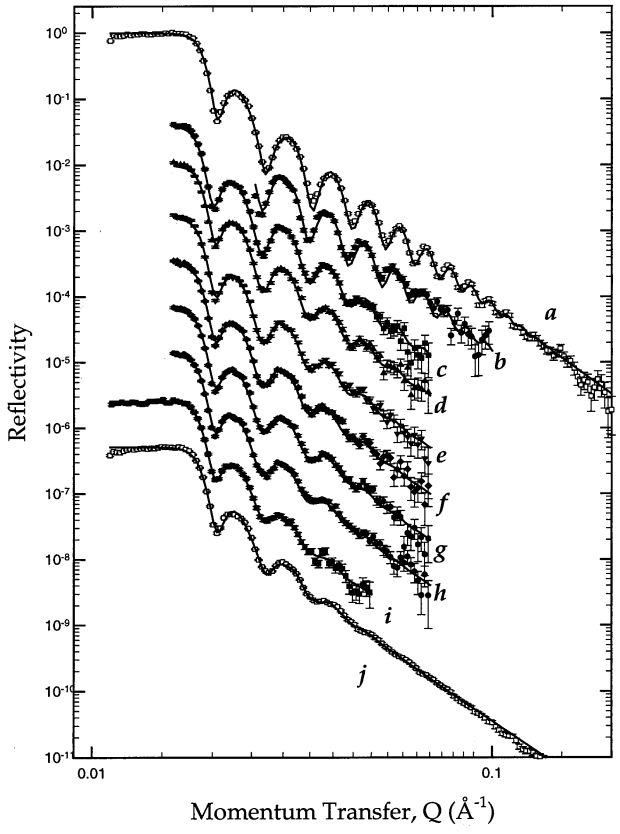

Figure 2. Reflectivity profiles for h-PS/d-PS bilayer. Measurements in real time at 115ºC (points), and solid lines are model fits to the data. Mean time for profiles plotted are (b) 5, (c) 32, (d) 63, (e) 93, (f) 124, (g) 155, (h) 186, (j) 212, measured for 6 min count times, (a) before annealing.

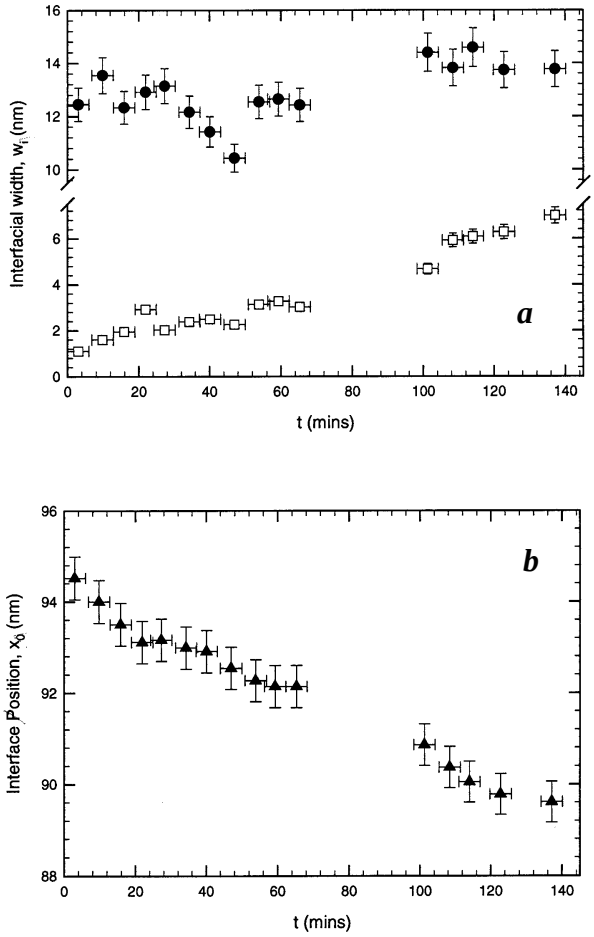

Figure 3. Variation of (***a***) interfacial width (w_1, w_2) and (***b***) position of interface (x_0) as a function of annealing time for OSt/d-PS.

interface is larger than that on the OSt side, confirming that the oligomer diffusion is much faster than the polymer diffusion. Both widths increase with time, and as expected the interface moves further into the d-PS with time.

Surfactant adsorption at interfaces

The nature of adsorption of surfactants at interfaces is important in the context of applications such as detergency, solubilization and emulsion stabilization. Of particular relevance to such applications is the adsorption of complex mixtures at interfaces. To understand the mechanisms involved in such applications, a knowledge of adsorbed amounts over a wide range of concentrations (from below to well in excess of the critical micellar concentration, cmc), and of the surface structure is required. With the selectivity and specificity provided by deuterium labelling, neutron reflectivity has been shown to be an ideal technique for such measurements, and its application in this area has recently been reviewed in detail by Lu *et al.*[8].

For a deuterated surfactant in null-reflecting water (nrw) (nrw, a 92 mole% H_2O/8 mole% D_2O mixture has a scattering length of zero, i.e. a refractive index identical to that of air) the reflected signal arises only from the adsorbed deuterated surfactant layer at the interface. The most direct way of determining the surface concentration of the surfactant is to fit the measured reflectivity profile by comparing it with a profile calculated using the optical matrix method[9,10] for a simple structural model. It is usually sufficient to assume that the surfactant is in the form of a single layer of homogeneous composition. The model pararmeter is then just the scattering length density, ρ, and the layer thickness, d. The area/molecule, A, in the adsorbed layer is then

$$A = b/\mathrm{d}\rho, \tag{5}$$

where b is the scattering length of the adsorbed molecule. It is straightforward to extend this method to the determination of the surface composition of a binary mixture. By selective deuteration of each component in turn the adsorbed amount of each component can be evaluated[11],

$$\rho = b_1/(A_1 d) + b_2/(A_2 d), \tag{6}$$

where b_i and A_i are now the scattering lengths and area per molecule of each component.

Figure 4 shows the adsorbed amounts of each component in the binary non-ionic surfactant mixture of monododecyl triethylene glycol ($C_{12}EO_3$) and monododecyl octaethylene glycol ($C_{12}EO_8$) at the air–water interface[12] obtained in such a way. Measurements were made for an equimolar mixture in the concentration range 10^{-5} to 10^{-2} M. Consistent with the theoretical predictions of Nikas *et al.*[13] there is an abrupt change in the monolayer composition at the cmc of the $C_{12}EO_3/C_{12}EO_8$ mixture. This abrupt change in composition in the monolayer is

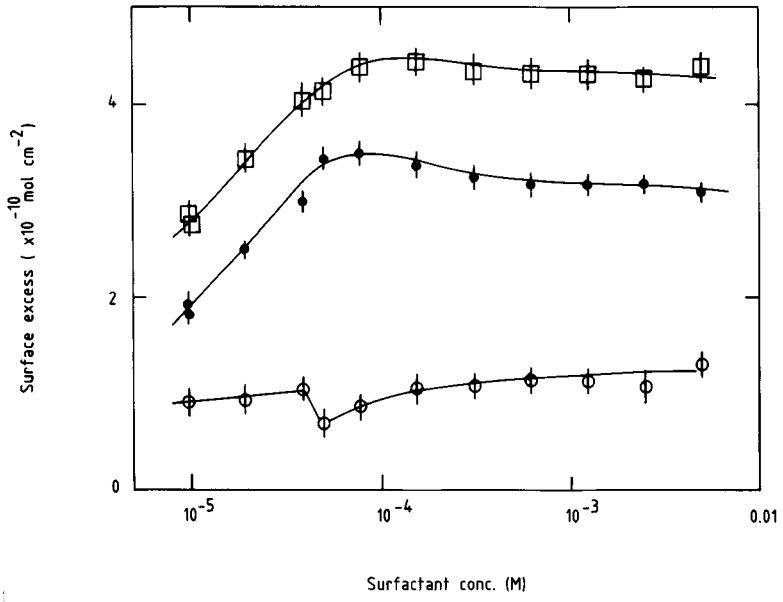

Figure 4. Adsorbed amounts, • ($\times 10^{-10}$ mol cm^{-2}) for an equimolar mixture of $C_{12}EO_3/C_{12}EO_8$ at the air–water interface (□), total; (•), $C_{12}EO_3$; and (o), $C_{12}EO_8$.

due to changes in the distribution of the two surfactant species between the bulk solution and the monolayer owing to the onset of mixed micelle formation at the cmc. These measurements provided the first experimental verification of the predictions of Nikas *et al.*[13]. Although close to ideal mixing, measurements with more detailed labelling showed that the structure of the mixed monolayer was different from that of the pure component monolayers[14].

In the simplest deuterium labelling scheme, by labelling either surfactant and solvent, the scattering length density profile can be written as,

$$\rho(z) = b_{C_{12}EO3}N_{C_{12}EO3}(z) + b_{C_{12}EO8}N_{C_{12}EO8}(z) + b_sN_s(z), \quad (7)$$

where N_i and b_i are the number density distribution and scattering lengths of the $C_{12}EO_3$, $C_{12}EO_8$ and solvent. Substituting into the expression for the reflectivity (eq. 1) we obtain,

$$R(Q) = \frac{16\pi^2}{Q^2}\begin{bmatrix} b^2_{C_{12}EO_3}h_{C_{12}EO_3} + b^2_{C_{12}EO_8}h_{C_{12}EO_8} + b_s^2h_s \\ +2b_{C_{12}EO_3}b_{C_{12}EO_8}h_{C_{12}EO_3}h_{C_{12}EO_8} \\ +2b_{C_{12}EO_3}b_sh_{C_{12}EO_3s} + 2b_{C_{12}EO_8}b_sh_{C_{12}EO_8s} \end{bmatrix}, \quad (8)$$

where h_{i1} are the self-partial structure factors given by

$$h_{ii}(Q) = |\hat{n}_1(Q)|^2, \quad (9)$$

and h_{ij} are the cross-partial structure factors given by

$$h_{ij}(Q) = R_e|\hat{n}_i(Q)\hat{n}_j(Q)|, \quad (10)$$

where $\hat{n}_i(Q)$ is the one-dimensional Fourier transform of $n_i(z)$. The self-partial structure factors relate to the distributions of the individual components and the cross-partial structure factors to the relative positions of the different components at the interface. It has been shown[15] that simple analytic functions can be used to describe these partial structure factors. The self terms, which describe the distribution of the individual components of the surfactant, can be described as a Gaussian distribution,

$$n_i(z) = n_{i0}\exp(-4z^2/\sigma^2), \quad (11)$$

which gives

$$h_{ii}(Q) = \frac{\pi\sigma_i^2n_{i0}^2}{4}\exp(-Q^2\sigma_1^2/8), \quad (12)$$

where n_{i0} is the number density of component i and σ the width of the distribution. For the solvent a tanh profile is used:

$$n_s(z) = n_{s0}(1/2 + 1/2\tanh(z/\zeta)), \quad (13)$$

where ζ is the width parameter and n_{s0} is the bulk solvent number density such that,

$$h_{ss}(Q) = n^2{}_{s0}(\zeta\pi/2)^2\,\mathrm{cosech}^2(\zeta\pi Q/2). \quad (14)$$

For the combination of even distributions and of even–odd distributions, the cross-partial structure factors have the simple relationships

$$h_{ij} = \pm(h_{ii}h_{jj})^{1/2}\cos(Q\delta_{ij}), \quad (15)$$

$$h_{is} = \pm(h_{ii}h_{ss})^{1/2}\sin(Q\delta_{is}), \quad (16)$$

where δ is the distance between the centre of the two distributions.

Taking, for example, the simple case outlined in eq. 8, six different measurements with different isotopically labelled components and solvent enable the six partial structure factors to be determined. Such a set of measurements provides some redundancy in the determination of the structure, as the 3 cross-terms (and hence the separations) are related such that,

$$\delta_{C_{12}EO_3C_{12}EO_8} = \delta_{C_{12}EO_3s} - \delta_{C_{12}EO_8s}. \quad (17)$$

The information content depends critically upon the actual labelling scheme used. For example, labelling an entire alkyl chain may not provide sensitivity to subtle changes in conformation, as the overall dimension may have a significant contribution from capillary wave broadening. The cross-terms are however unaffected by such factors[15].

Using partial deuterium labelling of the alkyl and ethylene oxide chains of $C_{12}EO_3$ and $C_{12}EO_8$ the structure of the mixed monolayer is compared with the pure $C_{12}EO_3$ and $C_{12}EO_8$ monolayers. In this case the outer C_6 of the alkyl chains were labelled to provide enhanced sensitivity to changes in the conformation of the alkyl chain. The frustration caused by the packing of the triethylene and octaethylene glycol headgroups results in a change of the surfactant structure compared to the pure monolayer of either surfactant. Compared to the pure monolayer the alkyl chain distributions of both surfactants are more extended, the triethylene glycol group is less hydrated, and the octaethylene glycol group is less extended, more hydrated (Figure 5).

Understanding the nature of solubilization at a molecular level is important in the widespread applications of solubilization, which include detergency, oil recovery, pesticides, cosmetics and food science. For example, the effects of adding short-chained alcohol are expected to be closely linked to its location within the interfacial region. Using partial deuterium labelling of different parts of the alkyl chain of hexadecyl trimethyl

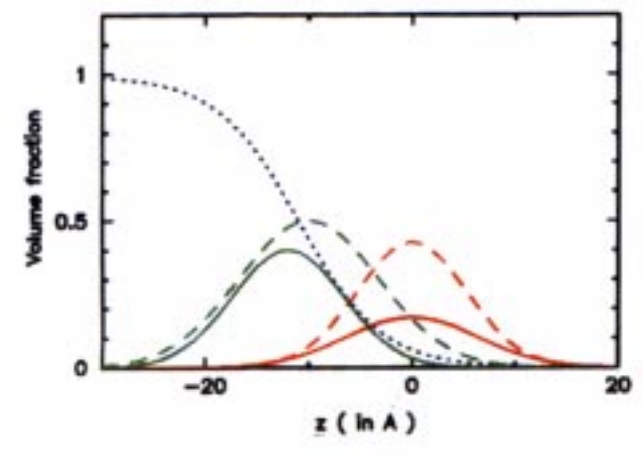

Figure 5. Volume fraction distribution for 30/70 mixture of $C_{12}EO_3/C_{12}EO_8$ at the air–water interface at 5×10^{-5} M, compared to a pure $C_{12}EO_8$ monolayer: (….), solvent; solid lines, $C_{12}EO_8$ in mixture; dashed lines, pure $C_{12}EO_8$ monolayer; red, outer C_6 of alkyl chain; green, EO_8.

ammonium bromide, C_{16}TAB, the distribution of benzyl alcohol molecules in a C_{16}TAB/benzyl alcohol mixed monolayer has been investigated[16]. For measurements with the outer C_{10} of the C_{16}TAB and the benzyl alcohol labelled in nrw we have,

$$R(Q) = \frac{16\pi^2}{Q^2}[b_{c1}^2 h_{c1c1} + b_{ba}^2 h_{baba} + 2b_{c1}b_{ba}h_{c1ba}], \qquad (18)$$

where *ba* and *c*1 refer to the benzyl alcohol and the outer C_{10} of the alkyl chain. Similar measurements for the C_6 adjacent to the C_{16}TAB headgroup enable the position of the benzyl alcohol at the interface relative to the C_{16}TAB alkyl chain (to an accuracy of ± 1 Å) to be determined. More extensive measurements provide a description of the conformation of the alkyl chain of the C_{16}TAB. The conformation of the C_{16}TAB molecule is not significantly altered by the addition of benzyl alcohol. However, the addition of benzyl alcohol draws the C_{16}TAB chain closer to the aqueous subphase; a similar change has been seen in other mixed monolayers. The distribution of the benzyl alcohol molecules in the interface is found to be centred on the 3rd methylene group in the headgroup of the alkyl chain of the C_{16}TAB (Figure 6).

Although measurements at the air–water interface are the most straightforward, the use of specular neutron reflection to study adsorption at the liquid–solid interface is now routine. The sample geometry used for measurements at the liquid–solid interface is for the neutron beam to be incident at glancing angles at the liquid–solid interface by transmission through a crystalline silicon upper phase[17]. Penfold *et al.*[18] have used the

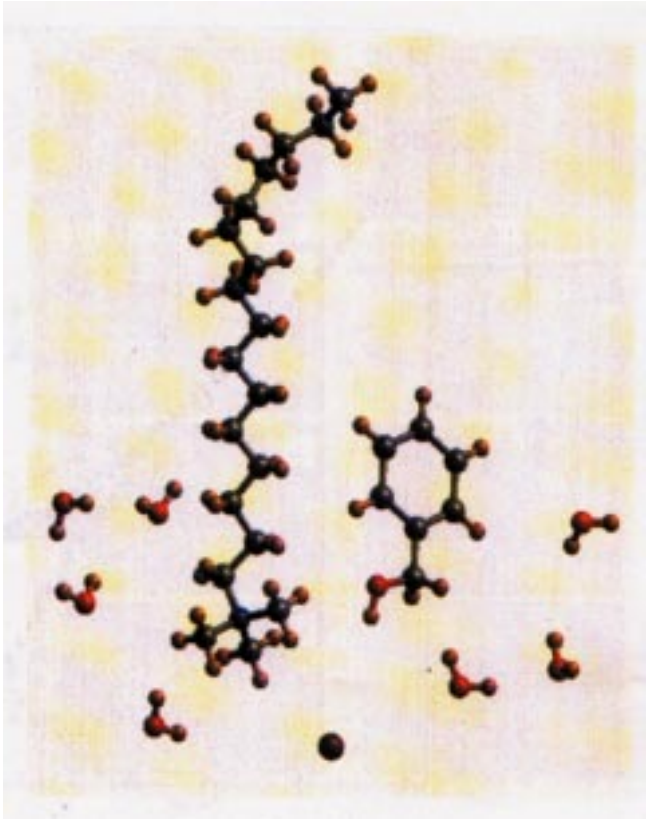

Figure 6. Schematic representation of the structure of the mixed C_{16}TAB and benzyl alcohol monolayer, showing the relative positions of the C_{16}TAB and benzyl alcohol molecules.

same deuterium labelling methods described earlier to study the adsorption of mixed surfactants at the hydrophillic silica–water interface. Figure 7 shows the measurements for a equimolar mixture of C_{16}TAB/$C_{12}EO_6$ at 10^{-4} M in 0.1 M NaBr/D_2O adsorbed at the Si/SiO_2 hydrophillic interface.

In this case the protonated surfactants provide an effective contrast against the deuterated solvent (D_2O). Measurements with both surfactants protonated give an estimate of the total adsorbed amount, whereas measurements with one or other component deuterated (where the deuterated component is effectively index matched to the solvent) provide information on the amount of each component at the interface. Not only is compositional information obtained, but the detailed surface structure of the adsorbed layer is determined. Measurements were made with differently labelled combinations of surfactants in D_2O, H_2O and in water index matched to silicon, cmSi. The simplest model that is consistent with all the data is a fragmented interdigitated bilayer. The nature of the interaction with the surface affects not only the composition of the adsorbed layer, but also the structure[18,19]. Measurements for the C_{16}TAB/$C_{12}EO_6$ mixture as a function of pH, show how

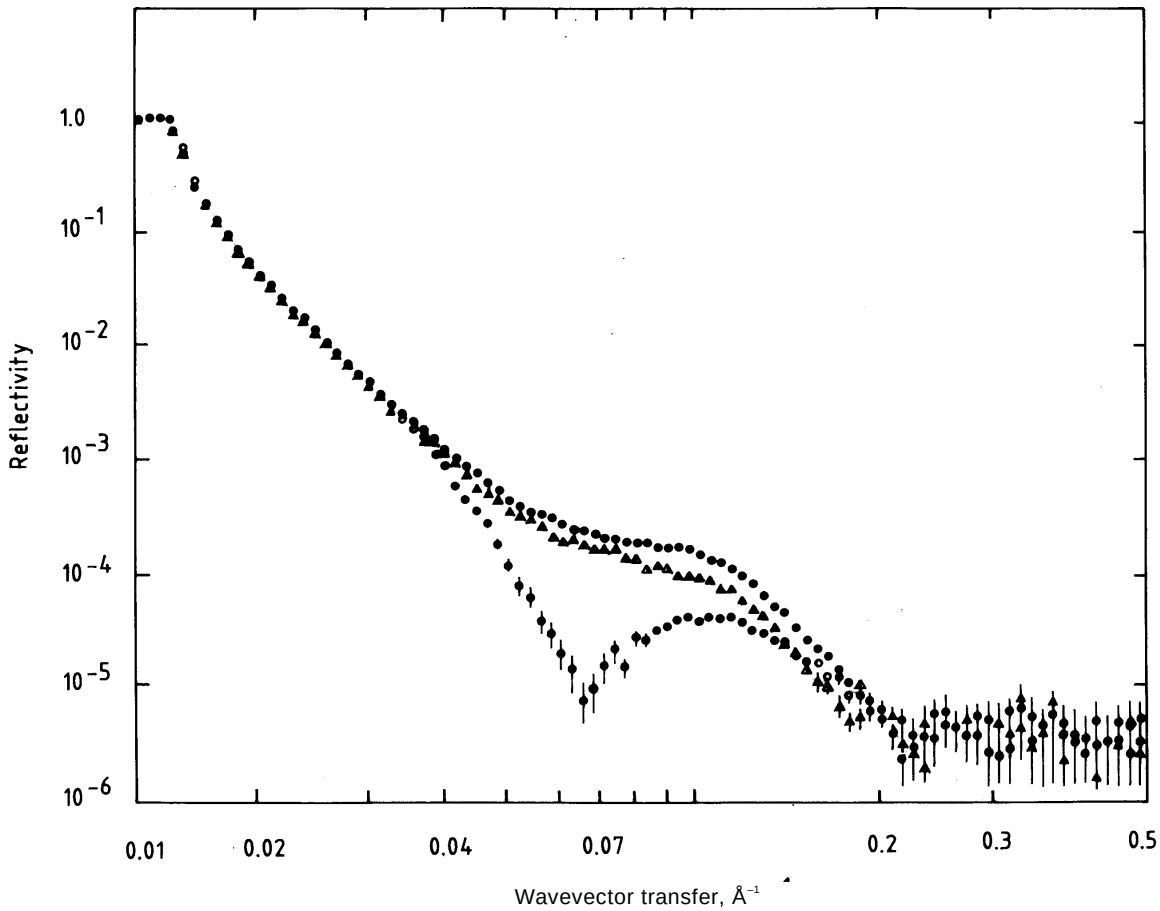

Figure 7. Specular reflection for equimolar mixture of $C_{16}TAB/C_{12}EO_6$ at 10^{-4} M in 0.1 M $NaBr/D_2O$ at the Si/SiO_2 hydrophilic interface. (o), h-$C_{16}TAB$/h-$C_{12}EO_6$; (•), h-$C_{16}TAB$/d-$C_{12}EO_6$; and (**s**), d-$C_{16}TAB$/h-$C_{12}EO_6$.

the relative affinity for adsorption of the two surfactants at the interface can dramatically alter the surface composition. Compared to the mixing at the air–water interface the specific interaction with the solid surface can have a profound effect on the surface mixing.

Protein adsorption at interfaces

The nature of protein adsorption at interfaces is important in the context of biocompatibility fouling and food emulsion stabilization. Lu and co-workers[20–23] have extensively studied the adsorption of two proteins, lysozyme and bovine serum albumim (BSA), at the air–water and liquid–solid interfaces. They have shown that it is not always necessary to deuterium label the adsorbed species. At the air–water interface for BSA and lysozyme in nrw they were able to show that there was sufficient contrast to obtain a reflectivity profile which provided an estimate of adsorbed amounts, and a layer thickness which could be interpreted in terms of a molecular conformation at the interface. Measurements with different water contrasts and especially with the solvent index matched to the protein provided additional information about the surface conformation, and in particular the extent of immersion of the protein layer in the underlying solvent. Measurements of lysozyme at the hydrophillic solid–liquid interface[22], for the solution in D_2O, give accurate determination of the adsorbed layer thickness, which in combination with known dimensions of the globular structure of lysozyme, provide direct evidence of the conformation of the protein at the interface. At low protein concentrations a monolayer thickness of 30 ± 2 Å was obtained, consistent with the long axis of the lysozyme being adsorbed parallel to the surface (side-ways on). Dependent upon pH the molecules tilt toward longways-on adsorption at higher concentrations, and ultimately form multilayers. Further conformational information is obtained for measurements in which the solvent contrast is varied. The results for both lysozyme and BSA are consistent with the proteins retaining their tertiary structure at the air–water and hydrophillic liquid–solid interfaces[22,23], but they are denatured at the hydrophobic liquid–solid interface[24].

The removal of proteins from interfaces by surfactants, although of considerable technological importance, is poorly understood. With this in mind Lu *et al.*[25] have studied the building of sodium dodecyl sulphate (SDS) to BSA layers adsorbed at the silica–water interface. The adsorption of BSA onto a hydrophillic silica surface produces a densely-packed uniform layer of thickness 35 ± 3 Å. The binding of SDS results in an expansion of the pre-adsorbed layer from 35 ± 3 Å in the absence of SDS to 50 ± 5 Å, suggesting a considerable structural deformation of the protein (Figure 8). Using deuterium-labelled SDS it is possible to determine the composition of the adsorbed complex. The weight ratio of SDS to BSA in the mixed layer was found to be 0.43, close to value for the binding of SDS to denatured protein in the bulk, suggesting that the protein in the adsorbed complex is also denatured.

Ordered silica films

The growth of highly ordered silicate structures, templated by lyotropic mesophases is an area of considerable current interest. White *et al.*[26] have used X-ray and neutron reflectivity to follow *in situ* the growth of highly ordered thin silicate-organic files at the air–water interface of surfactant solutions. In this case, the X-ray data provide an additional and crucial contrast required for the refinement of data modelling. C_{16}TAB and C_{16}TAC were used at concentrations ~70 times the cmc as the templating surfactants and tetraethoxysilane was used as the initiator. Measurements were made for deuterated C_{16}TAB(C) in nrw and C_{16}TAB(C) in D_2O. The kinetics of the silicate film formation was followed by making a series of 30 min measurements. The *in situ* X-ray and neutron reflectivity measurements at the early stages of growth show a slow development of structure in the top 100 Å of solution, which is consistent with a monolayer of surfactant at the air–water interface, a layer of partially silicated material, and an interdigitated surfactant bilayer or layer of cylindrical micelles ordered parallel to the surface. Following this induction period, a rapid crystallization occurs to give a highly ordered structure with a repeat distance of 45 Å perpendicular to the surface, and composed of alternating layers of surfactant and silicated material (Figure 9). The scattering length density profiles in Figure 9 are obtained from a simultaneous refinement of the X-ray and neutron reflectivity data, constrained to give a self-consistent model. The narrow Bragg diffraction peaks associated with later stages suggest that the final silicate film is highly ordered, and extends substantially into the bulk solution.

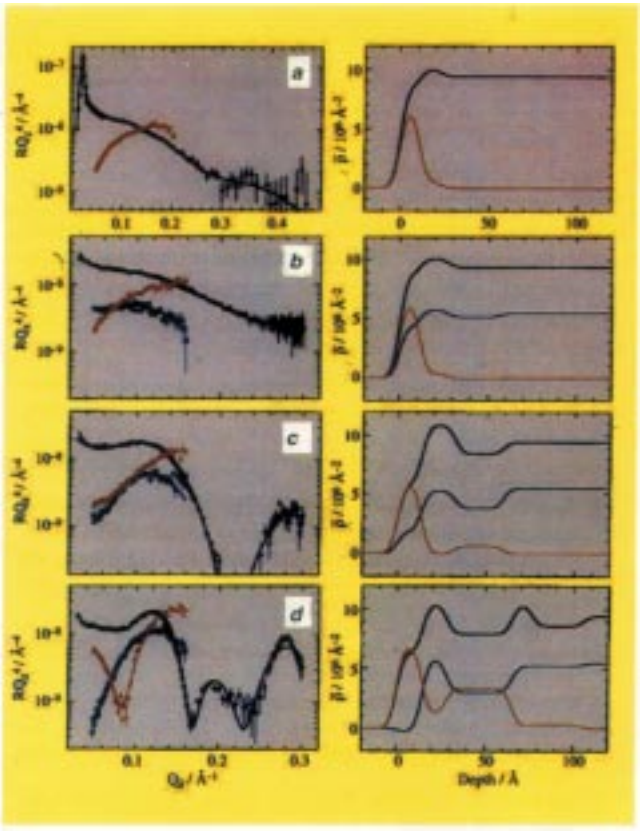

Figure 9. RQ^4 vs Q (left) and model scattering length density distributions (right) for ***a***, surfactant solution only; ***b–d***, for surfactant in silicate solution at 25, 75, and 90% of the time for Bragg peaks to appear. Black, h-C_{16}TAC/H_2O X-ray data; yellow, d-C_{16}TAB/nrw; and blue, h-C_{16}TAC/D_2O neutron data.

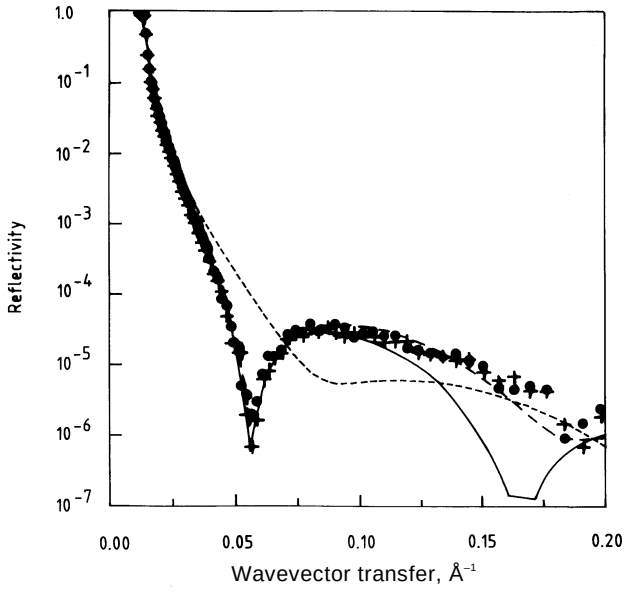

Figure 8. Specular reflectivity for binding of h-SDS to a pre-adsorbed BSA layer. (•), after 20 min; (+), 2 h, at the hydrophilic silica/D_2O interface. Dashed line (small) is for BSA only, the other two lines (solid line, large dashed line) are for uniform one and two layer models to the data.

Summary

The use of specular neutron reflection to study the structure of surfaces and interfaces has been illustrated for a wide range of problems in soft matter. The technique, in combination with H/D isotopic labelling, provides information for such systems which is difficult to obtain using other surface techniques. The examples cited in this review illustrate the development of the technique towards the study of complex mixtures, buried interfaces, the use of complex environments and the study of time-dependent phenomena.

1. Penfold, J. and Thomas, R. K., *J. Phys., Condens Matter*, 1990, **2**, 1369–1412.
2. Crowley, T. L., Lee, E. M., Simister, E. A. and Thomas, R. K., *Physica B*, 1991, **173**, 143.
3. Penfold, J., Richardson, R. M., Zarbakhsh, A., Webster, J. R. P., Bucknall, D. G., Rennie, A. R., Jones, R. A. L., Cosgrove, T., Thomas, R. K., Higgins, J. S., Fletcher, P. D. I., Dickinson, E., Roser, S. J., Mclure, I. A., Hillman, A. R., Richards, R. W., Staples, E. J., Burgess, A. N., Simister, E. A. and White, J. W., *J. Chem. Soc., Faraday Trans*., 1997, **93**, 3899–3917.
4. Penfold, J., Ward, R. C. and Williams, W. G., *J. Phys. E*, 1987, **20**, 1411–1417.
5. Russell, T. P., *Mater. Sci. Rep.*, 1990, **5**.
6. Xiao, C., Sferrazza, M., Jones, R. A. L., Bucknall, D. G., Webster, J. R. P. and Penfold, J., *Phys. Rev. Lett*., 1997, **78**, 3693–3696.
7. Bucknall, D. G., Butler, S. A. and Higgins, J. S., *Macromolecules*, 1999, in press.
8. Lu, J. R., Thomas, R. K. and Penfold, J., *Adv. Colloid Interface Sci*., 2000, 143–304.
9. Heavens, O. S., *Optical Properties of Thin Films*, Butterworths, London, 1955.
10. Penfold J., in *Neutron, X-ray and Light Scattering* (eds Zemb, T. and Lindner, P.), Elsevier, NY, 1991.
11. Simister, E. A., Thomas, R. K., Penfold, J., Aveyard, R., Binks, B. P., Fletcher, P. D. I., Lu, J. R. and Sokolowski, A., *J. Phys. Chem.*, 1992, **96**, 1383–1388.
12. Penfold, J., Staples, E., Thompson, L. and Tucker, I., *Colloid Surf*., 1995, **102**, 127–132.
13. Nikas, Y. F., Pruvvada, S. and Blankschtein, D., *Langmuir*, 1992, **8**, 2680–2688.
14. Penfold, J., Staples, E., Tucker, I. and Thomas, R. K., *J. Colloid Interface Sci*., 1998, **201**, 223–232.
15. Lu, J. R., Hromadova, M., Simister, E. A., Thomas, R. K. and Penfold, J., *J. Phys. Chem*., 1994, **98**, 11519–11526.
16. Penfold, J., Staples, E., Tucker, I., Soubiran, L., Lodi, A. K., Thompson, L. and Thomas, R. K., *Langmuir*, 1998, **14**, 2139–2144.
17. McDermott, D. C., Lu, J. R., Lee, E. M., Thomas, R. K. and Rennie, A. R., *Langmuir*, 1992, **8**, 1204–1210.
18. Penfold, J., Staples, E., Tucker, I. and Thompson, L., *Langmuir*, 1998, **13**, 6638–6643.
19. Penfold, J., Staples, E., Tucker, I., Thompson, L. and Thomas, R. K., *Int. J. Thermophys*., 1998, **20**, 19–34.
20. Lu, J. R., Su, T. J., Howlin, B. J. and Penfold, J., *J. Phys. Chem. B*, 1999, in press.
21. Lu, J. R., Su, T. J. and Penfold, J., *Langmuir*, 1999, in press.
22. Su, T. J., Lu, J. R., Thomas, R. K., Cui, Z. F. and Penfold, J., *J. Colloid Interface Sci*., 1998, **203**, 419–429.
23. Su, T. J., Lu, J. R., Thomas, R. K., Cui, Z. F. and Penfold, J., *J. Phys. Chem. B*, 1999, **103**, 3727–3738.
24. Fragneto, G., Thomas, R. K., Rennie, A. R. and Penfold, J., *Science*, 1995, **267**, 657–660.
25. Lu, J. R., Su, T. J., Thomas, R. K. and Penfold, J., *Langmuir*, 1998, **14**, 6261–6268.
26. White, J. W., Brown, A. S., Holt, S. A., Reynolds, P. A. and Penfold, J., *Langmuir*, 1998, **14**, 5532–5538.

ACKNOWLEDGEMENTS. I wish to acknowledge the work of the research groups of R. K. Thomas, J. R. Lu, J. S. Higgins and J. W. White that I have cited in this article and my collaboration with colleagues at Unilever Research and especially Ed Staples and Ian Tucker, and the contribution of my colleagues, John Webster, David Bucknall and Sean Langridge, at RAL.